# Evaluation of Grinding Wheel Surface by Means of Grinding Sound Discrimination*

Akira HOSOKAWA**, Kazufumi MASHIMO***,
Keiji YAMADA**** and Takashi UEDA†

In this study, a new technique of in-process evaluation of a grinding wheel surface is proposed. Some specific wheel surfaces are prepared as references by the appropriate truing and/or dressing procedure, and grinding sounds generated by these wheels are discriminated by analyzing the dynamic frequency spectrum by a neural network technique. In the case of a conventional vitrified-bonded alumina wheel, the grinding sound can be identified in the optimum network configuration. Therefore, this system can instantaneously recognize differences in the wheel surface with a good degree of accuracy insofar as the wheel conditions are relatively widely changed. In addition, the network can perceive wheel wear because the grain tips are flattened as grinding proceeds and the grinding sound becomes similar to that of a wheel generated with lower dressing feed. The resinoid-bonded cubic boron nitride (CBN) wheel is also discriminable when a grinding sound in a higher frequency range is analyzed.

***Key Words***: Grinding Wheel, Dressing, Surface Roughness, Grinding Sound, Neural Network, Discrimination

## 1. Introduction

In a grinding operation, machining accuracy and surface finish depend directly on the grinding wheel topography, i.e., the shape and distribution of cutting grains on the wheel surface. Therefore, several techniques have been developed concerning the measurement of wheel topography, such as profilometry, dynamometry and microscopy[1]-[4]. These methods are not, however, applicable to actual grinding operation because they require special instruments, much labor and time and have a tedious procedure. In addition, in-process measurement is actually desirable in a factory considering that the condition of a wheel surface is likely to change during the grinding process.

In this study, an in-process evaluation of the wheel surface is proposed, where the grinding sounds are analyzed by a neural network technique. The grinding sound generated by the wheel-workpiece interaction is one of the most valuable pieces of information reflecting the wheel conditions[5]. It is difficult, however, to quantify the geometrical or morphological characteristics of the wheel surface from the sonic signal at present. Hence, several conditions of the wheel surface —standard or reference conditions— are produced by appropriate truing and/or dressing and the characteristics of grinding sounds generated by these wheels are learned by the neural network. Then, based on the learned knowledge, the grinding sound from an arbitrarily dressed wheel is discriminated into one of the above references. Worn wheels are also evaluated by this method. In this report, two representative wheels —conventional vitrified-bonded alumina wheel and a resinoid-bonded cubic boron nitride (CBN) wheel— are chosen as targets.

## 2. Experimental Procedure

Plunge grinding of carbon steel at a constant

* Received 4th November, 2003 (No. 03-4154)
** Department of Mechanical Systems Engineering, Kanazawa University, 2-40-20 Kodatsuno, Kanazawa, Ishikawa 920-8667, Japan. E-mail: hosokawa@t.kanazawa-u.ac.jp
*** Mold Engineering Department, Toyoda Gosei Co., Ltd., 1 Komeyasakai, Kitajima, Inazawa, Aichi 492-8542, Japan. E-mail: tg25277@toyoda-gosei.co.jp
**** Department of Mechanical Systems Engineering, Kanazawa University, 2-40-20 Kodatsuno, Kanazawa, Ishikawa 920-8667, Japan. E-mail: kyamada@t.kanazawa-u.ac.jp
† Department of Mechanical Systems Engineering, Kanazawa University, 2-40-20 Kodatsuno, Kanazawa, Ishikawa 920-8667, Japan. E-mail: uada@kenroku.kanazawa-u.ac.jp

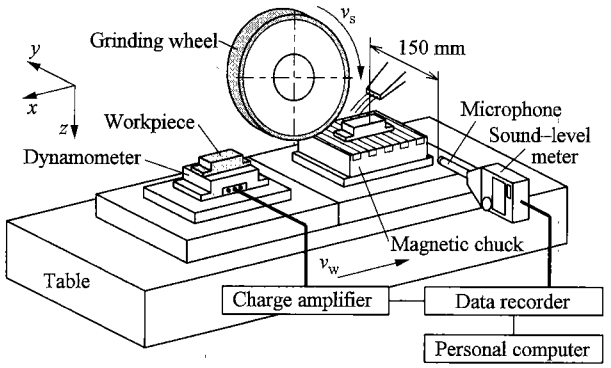


Fig. 1 Schematic of experimental arrangement

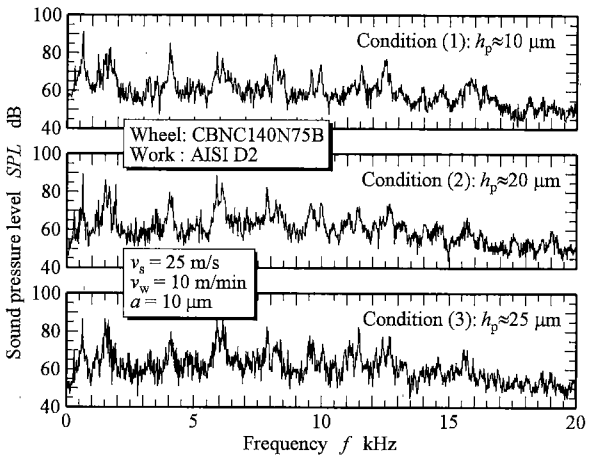


Fig. 2 Typical frequency spectra of the grinding sounds for three grinding wheel conditions

depth of cut is carried out. The experimental arrangement is illustrated schematically in Fig. 1. The grinding sound and grinding forces are measured using the noise-level meter and piezoelectric dynamometer, respectively. The microphone is set horizontally at a distance of 150 mm from the grinding point, as shown in Fig. 1. In order to avoid the vibration effect of the dynamometer, the grinding sound is recorded when the workpiece, which is fixed on the high-stiffness magnetic chuck (right specimen in Fig. 1), is ground. The practical procedure is as follows. First, some specific wheel surfaces are prepared as the references by the appropriate dressing. Secondly, the grinding sounds generated by these reference wheels are learned by the neural network, and finally the grinding sound from a redressed wheel is discriminated into one of the above references. It should be noted that the 'grinding sound' against the background of surrounding noise is detected in the actual situation.

## 3. Grinding Sound Discrimination by Means of Neural Network Technique

### 3.1 Network architecture

The frequency spectrums of the grinding sound emitted from the reference wheel surface are discriminated by the neural network learning algorithm. Figure 2 shows the typical frequency spectrum of the grinding sound for three reference conditions of the CBN wheel surface, in which the depth of the chip pocket is varied as described later. It is found, from the figure, that all spectrum curves have similar patterns showing some peaks due to the natural frequency of the system. According to this figure, it is obvious that we cannot distinguish these sounds aurally. The network program is constructed on the MATLAB® software package. It comprises a static (feed-forward) model which has a learning process in both hidden and output layers. The neural network structure used is presented in Fig. 3. The input signal is described as a column vector with $J$ elements of

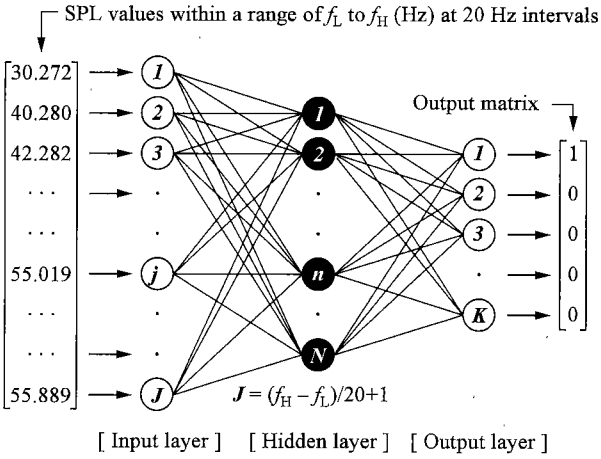


Fig. 3 Neural network structure

sound pressure level ($SPL$) values within an appropriate frequency range ($f_L$~$f_H$) at 20 Hz intervals. For instance, when $f_L$=10 kHz and $f_H$=15 kHz, $J$=(15−10)×10³/20+1=251. The analyzed frequency range is determined by convergence tests. The network also produces a column vector with $K$ elements. Here, $K$ is the number of reference conditions to be discriminated. The grinding sound is judged by the position of '1' on the $i$-th element in the output [$K$] column vector. In this experiment, multiple-layer networks are constructed and the learning algorithm comprises the error-back propagation (EBP) method[6] having the log-sigmoid transfer function.

### 3.2 Learning of grinding sound

In order to optimize the network architecture, it is necessary to determine the optimal learning rate $r_l$ and the number of neurons in hidden layer $N$ through learning experiments. In this study, the number of epochs required for network convergence is measured under various network configurations in which the number of neurons in the hidden layer $N$ and the

learning rate $r_l$ are changed in the ranges of 50 to 500 and 0.000 5 to 0.01, respectively. Learning stops when either the number of epochs attains a maximum value of 5 000 or the network sum-squared error drops below the error goal of 0.1. The parameters of the neural network configuration examined are listed in Table 1. Here, the number of cells in the input layer is determined from the frequency range of the grinding sound being analyzed and is $(f_H - f_L)/20 + 1$.

Figure 4 shows the learning result of the neural network as a mesh plot for the analysis of the grinding sound of the vitrified-bonded alumina wheel. As the diagram indicates, learning begins to converge when the number of neurons in hidden layer $N$ is more than about 100 and the number of epochs decreases as the number of neurons increases. In addition, higher the learning rate, the less time a network requires to be trained, but the learning does not converge when the learning rate exceeds a certain limit. On the whole, the grinding sound can be identified under the appropriate network configuration where the number of epochs is less than approximately 600.

Table 1 Parameters of neural network configuration

| | | |
|---|---|---|
| Structure | | Multiple layer network |
| Architecture | | Feed-forward network |
| Learning rule | | EBP |
| Number of hidden layers | | 1 |
| Neuron model | | Static analogue model |
| Transfer function | | Log-sigmoid |
| Number of neurons in input layer | $J$ | 201–251 |
| Number of neurons in hidden layer | $N$ | 50–500 |
| Number of neurons in output layer | | 3–5 |
| Learning rate | $r_1$ | $5\times10^{-4}$–$1\times10^{-2}$ |
| Maximum number of epochs | | 5000 |
| Error goal | | Sum-square error = 0 .1 |

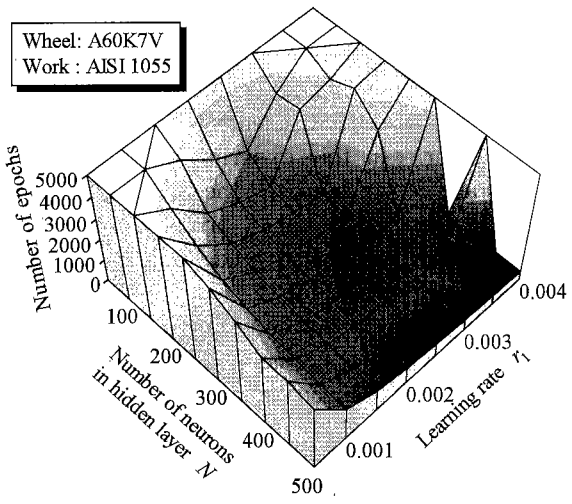


Fig. 4 Learning result of the neural network constructed

## 4. Conventional Vitrified-Bonded Alumina Wheel

### 4.1 Formation of the reference wheel surface

In the case of the conventional vitrified-bonded alumina wheel (A60K7V), the reference surfaces are formed by passing a single-point diamond dresser across the wheel at five dressing feed rates: $s_d$=10, 20, 50, 100 and 300 μm/rev as shown in Table 2. Here the values of $s_d$ are determined on the basis of the average grain diameter of the #60-wheel ($d_g \approx 250$ μm) so as to make fine to rough surfaces within the applicable range. The differences of the reference wheel surface are checked referring to grinding forces and surface roughness of the workpiece after plunge grinding. Figure 5 shows the variations of grinding force components ($F_t$, $F_n$) and arithmetic average roughness $R_a$ with dressing conditions. The symbols '○', '△' and '□' correspond to the results of reference wheels. It is found from the figure that five different surfaces of fine to rough conditions are generally formed, although there is no clear distinction in $R_a$ between two finest conditions (1) and (2). On the

Table 2 Dressing conditions of vitrified-bonded alumina wheel

| Condition No. $N_d$ | Dressing feed $s_d$ μm/rev | Condition No. $N_d$ | Dressing feed $s_d$ μm/rev |
|---|---|---|---|
| (1) | 10 | | |
| (2) | 20 | (23) | 35 |
| (3) | 50 | (34) | 75 |
| (4) | 100 | (45) | 200 |
| (5) | 300 | | |

Wheel speed: $v_s$ = 25 m/s
Dressing depth: $a_d$ = 10 μm (5passes)
Grinding fluid: Water-based solution (1:50) in water
Dresser: Single-point diamond dresser

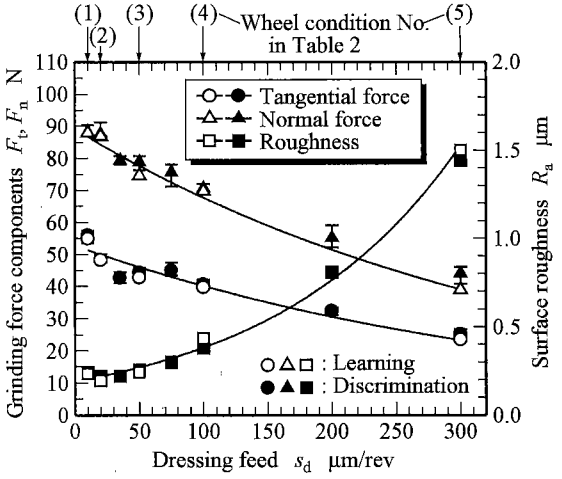


Fig. 5 Variations of grinding force components and surface roughness with dressing conditions

whole, it seems reasonable to say that these five conditions —(1), (2), (3), (4) and (5)— can be regarded as references, where the grinding ability differs in incremental steps within the practical range.

### 4.2 Experimental conditions and results

The plunge grinding of carbon steel (≈AISI 1055, 400HV20) at a constant depth of cut is executed. The experimental conditions are summarized in Table 3. Ten one-pass grinding tests are conducted for each redressed grinding wheel listed in Table 2, in which No. (23), (34) and (45) are those formed by intermediate dressing feed between (2) and (3), (3) and (4) and (4) and (5), respectively. These three conditions are untrained ones in the network. The variations of grinding force components (●, ▲) and surface roughness (■) are again plotted in Fig. 5. On the basis of the figure, it is reasonable to say that conditions similar to those of the references are formed with dressing conditions No. (1), (2), (3), (4) and (5), and also formed approximately intermediate ones between (2) and (3), (3) and (4) and (4) and (5) in the cases of dressing conditions No. (23), (34) and (45), respectively.

Table 4 shows the result of discrimination in the form of a confusion matrix, which is obtained by inputting 10 sounds for each wheel condition. The element $(i, j)$ of the matrix represents the number of outputs when the result of recognition is the $j$-th sound against the input of the $i$-th sound. It is found from the table that the position of the maximum value

Table 3 Grinding conditions

| | | | |
|---|---|---|---|
| Grinding wheel | | A60K7V | CBNC140N75B |
| Workpiece | | AISI 1055(400HV20) | AISI D2(800HV20) |
| Width | $b_w$ | 10 mm | 8 mm |
| Length | $l_w$ | 50 mm | |
| Operating parameters | | | |
| Wheel speed | $v_s$ | 25 m/s | |
| Work speed | $v_w$ | 10 m/min | |
| Depth of cut | $a$ | 10 μm | |
| Grinding fluid | | Water-based solution (1:50 in water) | |

Table 4 Results of grinding sound discrimination

| Input sound $N_d$ | Input sound $s_d$ (μm/rev) | Result of discrimination (Number of outputs in 10 experiments) (1) | (2) | (3) | (4) | (5) |
|---|---|---|---|---|---|---|
| (1) | 10 | 8 | 2 | 0 | 0 | 0 |
| (2) | 20 | 0 | 10 | 0 | 0 | 0 |
| *(23) | 35 | 0 | 0 | 9 | 1 | 0 |
| (3) | 50 | 2 | 0 | 8 | 0 | 0 |
| *(34) | 75 | 0 | 0 | 0 | 8 | 2 |
| (4) | 100 | 0 | 0 | 0 | 10 | 0 |
| *(45) | 200 | 0 | 0 | 0 | 3 | 7 |
| (5) | 300 | 0 | 2 | 0 | 0 | 8 |

*: Unlearned conditions $f_L = 6$ kHz, $f_H = 10$ kHz, $r_1 = 2.9\times10^{-3}$, $N = 420$

of number of outputs —which is masked by hatching — shows the correct discrimination and the overall recognition rate is at least 80% when the input sounds are those from the wheel dressed with the same conditions as the references (No. (1), (2), (3), (4) and (5)). Due to surrounding noise and other factors, some incorrect outputs are observed.

It must be noted that the results of discrimination of unlearned sounds No. (23), (34) and (45) reveal that when the grinding sound from a wheel other than any of the five learned references is input, the network indicates the nearest reference as the output, as shown in Table 4. Judging from the above results, we can estimate the wheel condition by analyzing the grinding sound of several passes, unless wheel topography changes drastically.

### 4.3 Sound recognition in the process of wheel wear

As Fig. 5 indicates, the grain tips seem to be flattened as the dressing feed decreases from $s_d$=300 to 10 μm/rev. On the other hand, cutting edges also become flat when attritious wear is dominant without falling-off and/or macroscopic fracture of abrasive grains in the grinding process. Based on the above consideration, the grinding sound discrimination tests are executed in long-term grinding operation in order to verify the flexibility of this network system. When the wheel is initially formed under dressing condition (4), the wheel surface seems to change to a condition equivalent to (1) as grinding proceeds, because of wheel wear.

Figure 6 shows the variations of grinding force components ($F_t$, $F_n$), surface roughness $R_a$ and radial wheel wear $\Delta R$ with accumulated stock removed $V_W$ when the initial wheel condition is No. (4) in Table 2. It is seen in the figure that both $F_t$ and $F_n$ increase as $V_W$ increases, and $\Delta R$ decreases with $V_W$. Judging from the values of $F_t$, $F_n$ and $R_a$ in Fig. 6, the wheel condition seems to change from No. (4) to No. (3)/No. (2).

Table 5 shows the result of discrimination in the same manner as Table 4, where the input sounds vary with stock removal volume $V_W$. It can be seen in the table that the position of maximum values of number of outputs in the output matrix shift from (4) to (3) as stock removal volume increases. This means that the grain tip is flattened, so that the grinding sound resembles that of the wheel generated with a lower dressing feed. The output, however, does not shift after $V_W$=50 mm$^3$, as shown in Table 5. The most plausible explanation for this results is as follows. This wheel consists of relatively fragile abrasives of soft grade; accordingly the localized micro-fracture of abrasives occurs simultaneously with attritious

wear.

Another experimental result is presented in Table 6, in which tougher grains are used although the wheel specifications are the same as those of A60K7V. Due to the dominant attritious wear, the discernment results shift from No. (4) to (2) via (3) with greater stock removed compared with the friable wheel shown in Table 5. From the above results, it can be said that the network is capable of recognizing wheel wear.

Table 5 Result of grinding sound discrimination in the process of grinding operation

| Input sound $V_w$ (mm$^3$) | Result of discrimination (Number of outputs in 10 experiments) (1) | (2) | (3) | (4) | (5) |
|---|---|---|---|---|---|
| 0 | 0 | 1 | 2 | 7 | 0 |
| 50 | 0 | 0 | 6 | 0 | 4 |
| 100 | 0 | 1 | 7 | 1 | 1 |
| 150 | 0 | 1 | 7 | 1 | 1 |
| 200 | 0 | 0 | 6 | 0 | 4 |
| 250 | 0 | 0 | 9 | 0 | 1 |

The initial wheel condition is (4): $s_d$ = 100 μm/rev

Table 6 Result of grinding sound discrimination in the process of grinding operation for a hard wheel with tough grains

| Input sound $V_w$ (mm$^3$) | Result of discrimination (Number of outputs in 10 experiments) (1) | (2) | (3) | (4) | (5) |
|---|---|---|---|---|---|
| 0 | — | 0 | 0 | 8 | 2 |
| 845 | — | 1 | 1 | 8 | 0 |
| 1690 | — | 1 | 0 | 8 | 1 |
| 2535 | — | 3 | 2 | 5 | 0 |
| 3380 | — | 4 | 6 | 0 | 0 |
| 4225 | — | 7 | 2 | 0 | 1 |
| 5070 | — | 6 | 4 | 0 | 0 |
| 6760 | — | 7 | 3 | 0 | 0 |

The initial wheel condition is (4): $s_d$ = 100 μm/rev

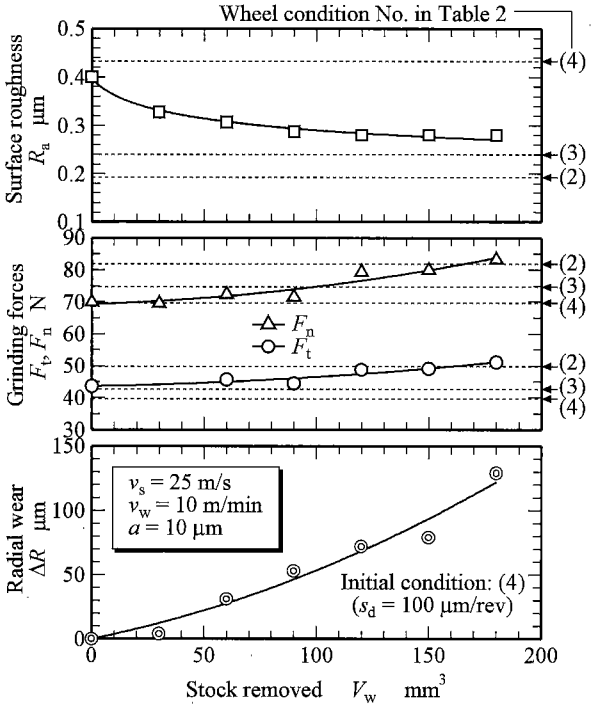


Fig. 6 Variations of grinding force components, surface roughness and radial wheel wear with accumulated stock removed

## 5. Resinoid-Bonded CBN Wheel

### 5.1 Formation of reference wheel surface and measurement of wheel topography

The applicability of this technique to the resinoid-bonded CBN wheel (CBNC140N75B) is also examined. Because of the nonporous bond, the wheel is first trued by the metal-bonded diamond block truer and then the bonding material is removed by dressing with the rotary WA-cup dresser so as to form an appropriate chip pocket, as shown in Fig. 7. After dressing, a profile trace along the circumference of the wheel is measured using a stylus coupled to a displacement transducer mounted on the grinding machine, as shown in Fig. 7, and the average depth of the chip pocket $h_p$ is calculated from the digitized profile data. Figure 8 shows a schematic illustration of a wheel profile, where abrasive grains and cutting edges are identified according to arbitrarily defined criteria. In the upper diagram, the area surrounded by the outermost wheel surface and the profile curve for each reference length $L_n$ is regarded as a chip pocket $S_n$, and $S_n/L_n$ is defined as the localized depth of the chip pocket. The peaks marked symbol '○' in the lower figure denote the identified cutting edges which have protrusion height over a certain value. Figure 9 shows the dressing characteristics where the relationship between the number of dressing passes and the

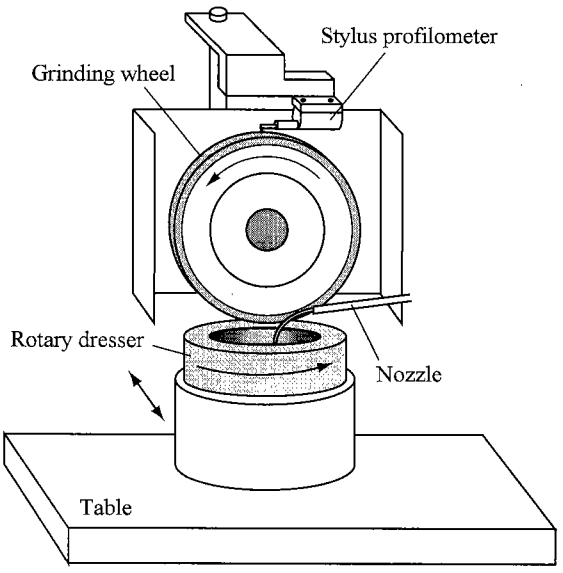


Fig. 7 Rotary dresser and stylus profilometer

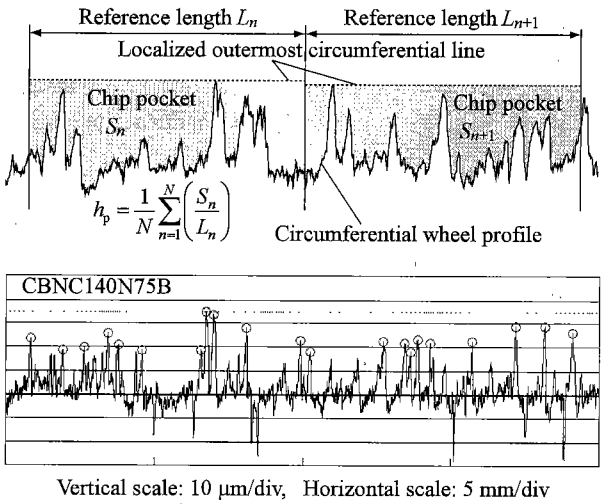


Fig. 8 Definition of average depth of chip pocket $h_p$ and typical wheel profile

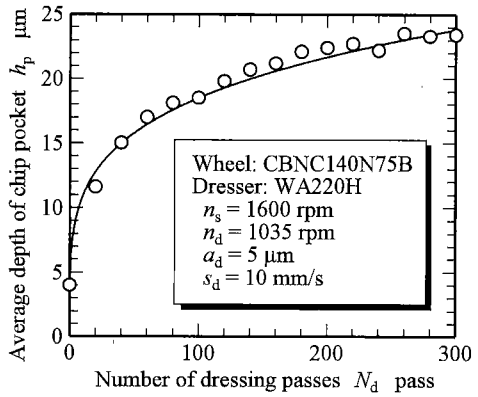


Fig. 9 Formation of chip pocket with dressing passes

depth of the chip pocket is indicated. Referring to this figure, the depth of chip pocket can be controlled by the dressing passes in a certain degree of accuracy.

In the case of the resinoid-bonded CBN wheel, three reference surfaces are prepared, as shown in Table 7, in which depth of chip pocket is set incremental steps as 10, 20 and 25 μm. Here the values of $h_p$ are determined by the average grain diameter of the wheel ($d_g \approx 100$ μm). It is difficult, however, to form a chip pocket with a completely accurate depth, so that the values of $h_p$ are slightly different between learning cases and discrimination ones. In this case, the micromorphology of abrasive grains are approximately the same under all conditions because abrasive grains are little damaged during dressing. The condition of the reference wheel surface is also checked on the basis of grinding forces and the surface roughness of the workpiece after plunge grinding, as presented in Fig. 10. The graph indicates (○, △, □) that the grinding characteristics of these three wheels differs suitably; therefore, these three conditions—(1), (2) and (3)—are reasonable as references.

Table 7 Three reference conditions of resinoid-bonded CBN wheel

| Condition No. $N_d$ | Average depth of chip pocket $h_p$ μm | | |
|---|---|---|---|
| | Target value | Learned value | Discriminated value |
| (1) | 10 | 10.4 | 9.9 |
| (2) | 20 | 20.1 | 19.8 |
| (3) | 25 | 25.3 | 24.1 |

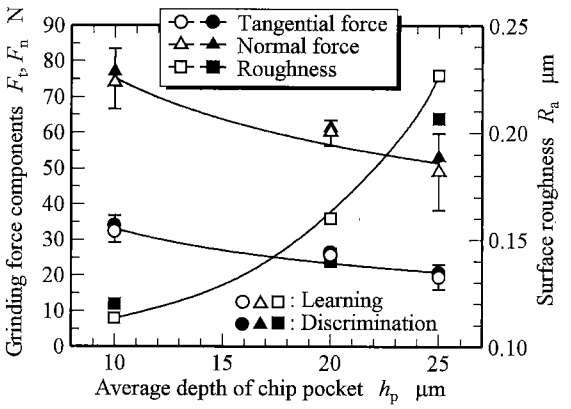


Fig. 10 Variations of grinding force components and surface roughness with depth of chip pocket for resinoid-bonded CBN wheel

### 5.2 Experimental conditions and neural network configuration

Grinding experiments of hardened die steel (≈AISI D2, 800HV20) are carried out in a similar way to that of the vitrified-bonded alumina wheel. The operating parameters are also listed in Table 3. The optimal learning rate and number of cells in the hidden layer are determined by learning experiments under various network configurations in which the number of cells in the hidden layer and the learning rate are changed in the range of 50 to 500 and 0.000 5 to 0.010, respectively. The learning result of the neural network is presented in Fig. 11 as a mesh plot. Compared with Fig. 4, it is obvious that learning converges in a wider range of $N$ and $r_l$; that is, the CBN wheel has more distinct grinding sound than the conventional alumina wheel in this case. As a result, the grinding sound can be well learned under the condition that learning rate is 0.0035 and number of neurons in the hidden layer is 350, as shown in Table 8, provided that the higher frequency range of 10 kHz to 15 kHz is analyzed.

### 5.3 Experimental results

Ten one-pass grinding tests are executed with a freshly dressed wheel, as listed in Table 7. In the experiments, the values of grinding forces and surface roughness are approximately the same as those for reference wheels shown in Fig. 10. Table 9 shows the results of discrimination in the form of a confusion

Table 8 Parameters of neural network configuration

| | |
|---|---|
| Learning frequency range | 10 – 15 kHz |
| Number of neurons in input layer $J$ | 251 |
| Number of neurons in hidden layer $N$ | 350 |
| Number of neurons in output layer | 3 |
| Learning rate $r_1$ | $3.5\times10^{-3}$ |
| Maximum number of epochs | 5000 |
| Error goal | Sum-square error = 0 .1 |

Table 9 Result of grinding sound discrimination for resinoid-bonded CBN wheel

| Input sound | | Result of discrimination (Number of outputs in 10 experiments) | | |
|---|---|---|---|---|
| $N_d$ | $h_p$ μm | (1) | (2) | (3) |
| (1) | 10 | 10 | 0 | 0 |
| (2) | 20 | 0 | 10 | 0 |
| (3) | 25 | 0 | 0 | 10 |

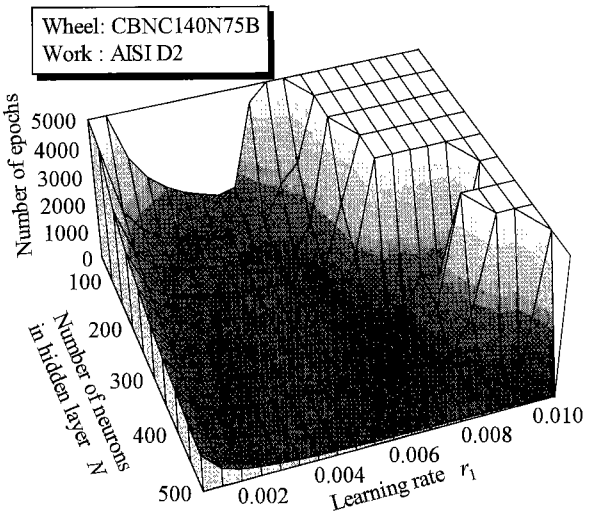


Fig. 11 Learning result of the neural network constructed

matrix, which is obtained by inputting 10 sounds for each wheel conditions in the same manner as shown in Table 4. It is found from the table that the grinding sound is perfectly discriminated into the equivalent reference condition. This is because the characteristics of the grinding sound of the CBN wheel are more sensitive to the wheel condition compared to those of the conventional alumina wheel. When the lower frequency range of grinding sound, however, is analyzed, the network cannot accurately distinguish the sounds of $h_p$=10 and 20 μm. One of the reasons for this result is that the micromorphologies of abrasive grains are similar between the two cases in so far as the microscopic observation. The discriminating ability of this technique of cutting-edge conditions should be investigated hereafter. In any case, there is room for further investigation of the optimization of the neural network architecture as well as of the frequency range to be analyzed, in order to evaluate the wheel surface more finely and accurately.

## 6. Conclusions

Practical monitoring system of a grinding wheel surface is developed. This system enables in-process evaluation of the wheel surface. In this dynamic measurement, the characteristics of the wheel surface are discriminated on the basis of the dynamic frequency spectrum signals of grinding sound using a neural network technique. In the given experiment, the network can discriminate the condition of the wheel surface to a good degree of accuracy under the optimum network configuration. Accordingly, this system can instantaneously recognize differences of the wheel surface for both a conventional vitrified-bonded alumina wheel and a superabrasive CBN wheel, insofar as the wheel topography is relatively widely changed by truing and/or dressing procedure.

## Acknowledgments

The authors are indebted to Mizuho Co., Ltd. and Noritake Super Abrasive Co., Ltd. for providing the alumina wheels and superabrasive wheels, respectively. We also wish to thank Nippon Grease Co., Ltd. for proffering the grinding fluids.

## References

(1) Verkerk, J., Final Report Concerning CIRP Cooperative Work on the Characterization of Grinding Wheel Topography, Annals of the CIRP, Vol. 26, No. 2 (1977), pp. 385-395.

(2) Hosokawa, A., Yasui, H. and Nagae, M., Characterization of Grinding Wheel Surface by Means of Image Processing, CESA'96 IMACS Multiconference, (1996), pp. 428-432.

(3) Besuyen, A.M., The Measurement of the Grinding Wheel Wear with the Quantimet Image Analyzing Computer, Annals of the CIRP, Vol. 19, No. 1 (1971), pp. 619-624.

(4) Hosokawa, A., Sakuma, K. and Takashi, U., In Situ Characterization of Grinding Wheel Surface, Proc of 14th Amer. Soc. Prec. Engg. Annual Meeting, Vol. 20, (1999), pp. 99-102.

(5) Higuchi, M., Yano., A, Ide, K., Kizu, S. and Komatsu, T., Diagnosis of Redress Life on Human Perception of Sound —Study on the Grinding Sound (3rd Report)—, J. Japan Soc. Prec. Eng., (in Japanese), Vol. 53, No. 12 (1987), pp. 1908-1912.

(6) Uesaka, Y., Fundamental Mathematics for Neurocomputing, (in Japanese), (1997), Kindaikagakusha.